Journal Pre-proofs

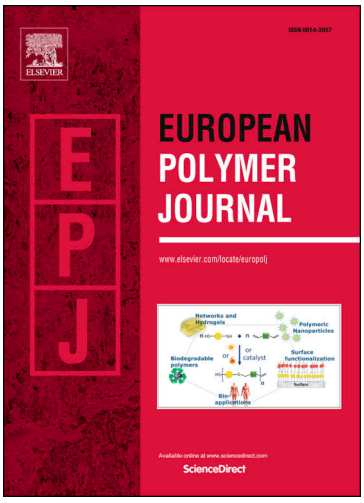

Sulfur's Role in the Flame Retardancy of Thio-Ether–linked Hyperbranched Poly(phosphoesters) in Epoxy Resins

Alexander Battig, Jens C. Markwart, Frederik R. Wurm, Bernhard Schartel

PII: S0014-3057(19)31924-X
DOI: https://doi.org/10.1016/j.eurpolymj.2019.109390
Reference: EPJ 109390

To appear in: *European Polymer Journal*

Received Date: 20 September 2019
Revised Date: 26 November 2019
Accepted Date: 27 November 2019

Please cite this article as: Battig, A., Markwart, J.C., Wurm, F.R., Schartel, B., Sulfur's Role in the Flame Retardancy of Thio-Ether–linked Hyperbranched Poly(phosphoesters) in Epoxy Resins, *European Polymer Journal* (2019), doi: https://doi.org/10.1016/j.eurpolymj.2019.109390

Sulfur's Role in the Flame Retardancy of Thio-Ether–linked Hyperbranched Poly(phosphoesters) in Epoxy Resins

Alexander Battig,[a,‡] Jens C. Markwart,[b,c,‡] Frederik R. Wurm,*[,b] and Bernhard Schartel*[,a]

[a] Bundesanstalt für Materialforschung und -prüfung (BAM), Unter den Eichen 87, 12205 Berlin, Germany.

[b] Max Planck Institute for Polymer Research, Ackermannweg 10, 55128 Mainz, Germany.

[c] Graduate School Materials Science in Mainz, Staudinger Weg 9, 55128 Mainz, Germany.

[‡] these authors contributed equally

* corresponding authors:

Bernhard Schartel, Bundesanstalt für Materialforschung und -prüfung (BAM), Unter den Eichen 87, 12205 Berlin, Germany. bernhard.schartel@bam.de;

Frederik R. Wurm, Max-Planck-Institut für Polymerforschung, Ackermannweg 10, 55128 Mainz, Germany. wurm@mpip-mainz.mpg.de

Abstract:

Hyperbranched poly(phosphoesters) are promising multifunctional flame retardants for epoxy resins. These polymers were prepared via thiol-ene polyaddition reactions. While key chemical transformations and modes of actions were elucidated, the role of sulfur in the chemical composition remains an open question. In this study, the FR-performance of a series of phosphorus-based flame retardant additives with and without sulfur (thio-ethers or sulfones) in their structure are compared. The successful synthesis of thio-ether or sulfone-containing variants is described and verified by ^{1}H and ^{31}P NMR, also FTIR and MALDI-TOF. A decomposition process is proposed from pyrolytic evolved gas analysis (TG-FTIR, Py-GC/MS), and flame retardancy effect on epoxy resins is investigated under pyrolytic conditions and via fire testing in the cone calorimeter. The presence of sulfur increased thermal stability of the flame retardants and introduced added condensed phase action. Likely, sulfur radical generation plays a key role in the flame-retardant mode of action, and sulfones released

incombustible SO_2. The results highlight the multifunctionality of the hyperbranched polymer, which displays better fire performance than its low molar mass thio-ether analogue due to the presence of vinyl groups and higher stability than its monomer due to the presence of thio-ether groups.

Keywords: Phosphoester; Hyperbranched; Sulfur; Thio-Ether; Flame Retardant; Epoxy Resin;

1. Introduction:

Polymeric flame retardants (FRs) based on phosphorus (P) are gaining increased attention,[1] not only because they more closely adhere to the requirements of REACH, but particularly due to their ability to mitigate some of the drawbacks of low molar mass variants, e.g. leaching or blooming out of the matrix, which diminish material properties such as glass-transition temperature (T_g). Especially hyperbranched (hb) polymers have been recently investigated, as these materials act as multifunctional FRs in polymer resins, thereby exhibiting good miscibility, low impact on T_g, and effective flame retardancy at low loadings.[2] Hyperbranched polymers may be produced in a one-pot synthesis, as opposed to the highly symmetrical dendrimers;[3] this ease of synthesis is a major contributor to the use of these complex-shaped polymers in a wide array of fields.[4, 5] The choice of reaction type is highly relevant to the material properties and application, and a wide range of synthetic approaches have been described.[6, 7] Previously, P-based A_3-type hb-polymers were synthesized,[8] and their efficacy as FRs for bisphenol A-based epoxy resins (EPs) was proven.[9] Another approach to attain P-based hb-polymers is via an A_2+B_3-type reaction: in previous work, P-based polymeric hyperbranched FRs (hb-FRs) were synthesized and their efficacy as additive FRs in bisphenol A-based epoxy resins (EPs) were demonstrated.[10] The hb-FRs were synthesized via thiol-ene polyaddition using ethanedithiol as an A_2-unit and low molar mass P-based FRs with systematically varied P-O and P-N contents as B_3-units. These low molar mass FRs were previously synthesized and investigated as additives in EP.[11] Research into the low molar mass FRs and their hb-polymeric variants indicated that conversion to polymers generally improved thermal stability and decreased impacts on T_g. However, the comparison between hb-polymers and their monomers did not fully consider the role of the sulfur (S)-containing A_2-component and how its presence may affect flame retardancy.

In this work, the role of S-containing compounds, i.e. thio-ethers and sulfones, in the flame retardancy of P-based FRs has been investigated to gain a better understanding of the impact of the A_2-linker of hb-FRs. Two S-containing low molar mass P-FRs are synthesized and their performance as additives in bisphenol-A-based EPs are compared to that of the previously synthesized hb-FR (**hbPPE**) and its non-

S-containing monomer (**mPE**). To better compare the performance of low molar mass FRs to that of **hbPPE**, a thio-ether-containing compound (**mPE-S**) was prepared via thiol-ene reaction of **mPE** with ethanethiol. Additionally, **mPE-S** was oxidized to form a sulfone-containing compound (**mPE-S-ox**).

The use of sulfur in flame retardancy has been investigated for a wide array of flame retardants and polymers. The role of sulfur oxidation was investigated for P-esters in bisphenol A, where it was found that flame retardancy increased with increasing levels of oxidation state.[12] Several S-containing FRs have been previously investigated in polycarbonates (PC), many of them as aromatic sulfonate salts.[13] Although the flame-retardant modes of action are not completely clear, one investigation stipulated that Fries-rearragement was accelerated by aromatic sulfonates in PC, causing higher cross-linking but a faster decomposition.[14] Moreover, extensive investigations into the flame-retardant action of elemental sulfur, sulfides, and disulfides were performed, highlighting that these compounds decompose to form sulfur radicals, which may promote cross-linking reactions.[15, 16] Sulfone-containing FRs were shown to release sulfur dioxide into the gas-phase,[17] which acts not only as a fuel-diluent thus reducing the combustion efficiency, but was shown to act as a radical-scavenger.[18, 19] Additionally, P-containing sulfones have been investigated as a toughening agent and flame retardant for epoxy resins.[20] Other S-based FRs include sulfamic acid-based salts, i.e. ammonium sulfamate, or diammonium imidobisulfonate, which proved as effective FRs for cotton and wool,[21] polyamide 6,[22, 23] and polymethyl methacrylate or polystyrene.[24] Furthermore, P and S-containing FRs have also been investigated in PC[25] and in thermoplastic polyurethanes.[26]

By analyzing the difference between S- and non-S-containing low molar mass FRs, new light may be shed on the role that S plays in effective flame retardancy of hb-FRs. Furthermore, by assessing the flame-retardant action of S-containing low molar mass FRs (S-FRs), additional information on the mode of action of hb-FRs may be gained, thus potentially helping improve future formulations.

2. Materials and Methods

Table 1. Material abbreviation, names, chemical structures, and calculated phosphorus content.

Abbreviation	Name	Chemical structure	P-content (calc.)
mPE	Tri(hex-5-en-1-yl)phoshate	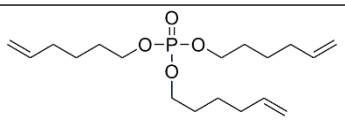	9.0 wt.-%
mPE-S	Tris[6-(ethyl thio)hexyl]phoshate	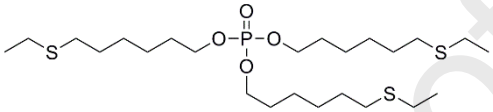	5.8 wt.-%
mPE-S-ox	Tris[6-(ethyl sulfonyl)hexyl]phoshate	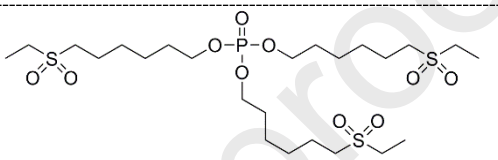	4.9 wt.-%
hbPPE	*hb*-Poly(phosphate)	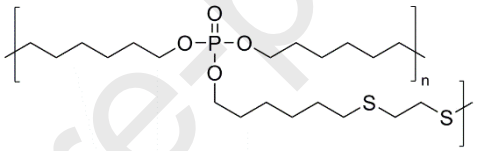	7.0 wt.-%
BDP	Bisphenol A bis(diphenyl phosphate)	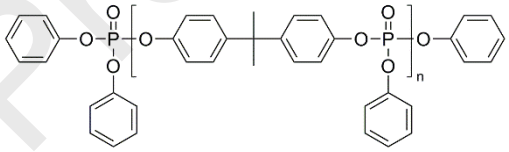	8.5 wt.-%
DGEBA	Diglycidyl ether of bisphenol A	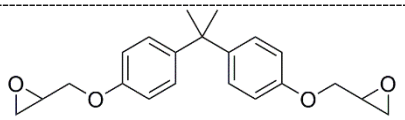	-
DMC	2,2'-dimethyl-4,4'-methylene-bis-(cyclohexylamine)	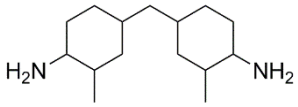	-

All chemicals were purchased from commercial suppliers as reagent grade and used without further purification. Bisphenol A bis(diphenyl phosphate) (BDP) was supplied by Albemarle (Louvain-la-Neuve, Belgium). Diglydyl ether of Bisphenol A (DGEBA, Araldite MY740) was supplied by Bodo Müller Chemie GmbH (Offenbach am Main, Germany). 2,2'-Dimethyl-4,4'-methylene-bis-(cyclohexylamine) (DMC) was purchased from Merck KgaA (Darmstadt, Germany).

2.1. Syntheses

mPE, hbPPE

mPE was prepared as previously described,[11] by the reaction of phosphoryl chloride with 5-hexene-1-ol. hbPPE was prepared as previously described,[10] where **mPE** was allowed to react with 1,2-ethanedithiol using azobisisobutyronitrile (AIBN) as an initiator.

mPE-S

mPE (56.5 g; 164.0 mmol; 1.0 eq.) was added to a dried 250 mL, round-bottomed flask under an argon atmosphere. Then, ethanethiol (48.5 mL; 656.2 mmol; 4.0 eq.) was slowly added while stirring the solution and cooling the flask with a water bath at room temperature. After a few minutes AIBN (808.1 mg; 4.9 mmol; 0.03 eq.) was added and the mixture was stirred overnight at 40 °C. The crude mixture was concentrated at reduced pressure to give a yellowish oil in quantitative yields.

^{1}H NMR (300 MHz, Chloroform-*d,* δ): 4.01 (q, *J* = 6.7 Hz, 6H), 2.51 (q, *J* = 7.3 Hz, 12H), 1.68 (dd, *J* = 12.9, 6.2 Hz, 6H), 1.63 – 1.51 (m, 6H), 1.39 (s, 12H), 1.24 (t, *J* = 7.4 Hz, 9H). (Figure S1)

^{31}P {H} NMR (121 MHz, Chloroform-*d,* δ): -0.67 (s, 1P). (Figure S2)

mPE-S-ox

mPE-S (33.0 g; 62.2 mmol; 1.0 eq.), dissolved in *N,N*-dimethylformamide (DMF) (125 mL), was added to a 250 mL, round-bottomed flask. Then, $B(OH)_3$ (82.9 mg; 1.2 mmol; 0.02 eq.) and 35% H_2O_2 (55 mL; 621.7 mmol; 10.0 eq.) were added while stirring the solution and cooling the flask with a water bath. The reaction was allowed to continue over night at 75 °C. The crude mixture was transferred to a separation funnel, where dichloromethane (DCM) and water were added. The water phase was washed two more times with DCM and the combined organic layers were washed with NaHCO3 solution, 10% aqueous hydrochloric acid solution and brine. The organic layer was dried over magnesium sulfate, filtered and concentrated at reduced pressure to give a white wax in quantitative yields.

^{1}H NMR (300 MHz, Chloroform-*d,* δ): 4.00 (q, J = 6.6 Hz, 6H), 2.95 (q, J = 7.4 Hz, 12H), 1.82 (dd, J = 6.4, 5.7 Hz, 6H), 1.68 (dd, J = 6.6 Hz, 6H), 1.43 (m, 12H), 1.37 (t, J = 7.5 Hz, 9H). (Figure S3)

^{31}P {H} NMR (121 MHz, Chloroform-*d,* δ): -0.71 (s, 1P). (Figure S4)

MALDI-TOF: 627.25 $[M+H]^+$, 649.24 $[M+Na]^+$, 665,21 $[M+K]^+$ (Calculated M^+ : 626.24).

Sample preparation

Epoxy resin samples were prepared in the following manner: DGEBA was placed into in a 1 L polypropylene cup and, where applicable, the FR (10 wt.-% loading) was added. With a wooden spatula, the mixture was blended until homogenous. DMC was then added next, then all components were stirred until fully mixed. Finally, the contents were poured into prepared aluminum molds. For cone calorimeter measurements, samples sized 100 mm x 100 mm x 4 mm were used.

2.2. Methods

^{1}H, ^{31}P {H} and ^{13}C {H} nuclear magnetic resonance (NMR) spectra were recorded with Bruker Avance spectrometers operating with 250, 300, 500, and 700 MHz frequencies in deuterated chloroform or deuterated dimethyl sulfoxide as a solvent. The calibration of the spectra was done against the solvent signal. The spectra were analyzed using MestReNova 9 from Mestrelab Research S.L.

Matrix-assisted laser desorption/ ionization – time of flight (MALDI–TOF) measurements were carried out with a Reflex I mass spectrometer (Bruker, Bremen, Germany), equipped with a 337 nm nitrogen laser. The spectra were recorded in the linear mode with the Bruker HIMAS detector at an acceleration voltage of 30 kV. 2-[(2*E*)-3-(4-*tert*-butylphenyl)-2-methylprop-2-enylidene]malononitrile (DCTB) was used as a matrix. To avoid fragmentation in MALDI–TOF mass spectrum (MS) measurements, the laser power required for the desorption/ionization process was carefully adjusted slightly above threshold.

A TG 209 F1 Iris (Netzsch Instruments, Selb, Germany) was used for thermographic analysis (TGA) measurements. A CryoMill (RETSCH, Germany) was used to mill epoxy resin-based samples into powder under liquid nitrogen. Pure FR samples (5 mg) or powdered polymer samples (10 mg) were heated at a constant heating rate (10 K min^{-1}) from 30 – 900 °C under a nitrogen flow (30 mL min^{-1}). A Fourier transform infrared spectrometer Tensor27 (Bruker Optics, Ettlingen, Germany) was used for evolved gas analysis of TGA samples (TG-FTIR). A heated (270 °C) transfer line connected TGA with FTIR. A Vertex70 FTIR spectrometer (Bruker Optics, Ettlingen, Germany) with an attached FTIR600 hot-stage cell (Linkam Scientific Instruments Ltd., Chilworth, UK) was used to measure condensed phase FTIR (range: 4000 – 40 cm^{-1}; resolution 0.4 cm^{-1}). Samples (5 mg) were mixed with potassium bromide (150 mg) and pressed into a platelet (pressure: 7 t). Under a constant heating rate (10 K min^{-1}) and constant nitrogen flow (300 ml min^{-1}), the platelets were heated from 30 – 600 °C.

A PY3030iD micro-furnace single-shot pyrolyzer (Frontier Laboratories, Japan) coupled via a split/ splitless inlet port to a 7890B gas chromatograph (Agilent Technologies, USA) and combined with a 5977B mass selective detector (Agilent Technologies, USA) was used to measure pyrolysis gas chromatography – mass spectrometry (Py-GC/MS). The mass spectrometer detector (ionization energy = 70 eV) had a scan range of 15 – 50 amu. Samples (150 µg) were pyrolyzed (500 °C) via gravimetric fall

into the pyrolysis zone under helium atmosphere. Using an Ultra Alloy +-5 capillary column (length = 30 m; inner diameter = 0.25 mm; film thickness = 0.25 µm), evolved pyrolysis products were separated under a constant flow of helium (1 mL min^{-1}). The column temperature ran for 2 min at 40 °C, then heated (10 K min^{-1}) to 300 °C and held for 10 min. The gas chromatograph injector (T = 300 °C) ran a split of 1:300. Peak assignments and product identification were done with the aid of the NIST 14 MS library.

A microscale combustion calorimeter (Fire Testing Technologies Ltd., East Grinstead, UK) was used for pyrolysis flow combustion calorimetry (PCFC) measurements. At a constant heating rate (1 K s^{-1}) and constant gas flow (nitrogen: 80 mL min^{-1}; oxygen: 20 mLl min^{-1}), powdered samples (5 mg) were pyrolyzed from 150 – 750 °C, and the evolved gases were combusted at 900 °C.

A Netzsch 204 FR "Phoenix" (Netzsch Instruments, Selb, Germany) was used to measure differential scanning calorimetry (DSC). Samples from the bulk material (5 mg) were measured at a constant heating / cooling rate (10 K min^{-1}) from -80 – 180 °C. Three heating and two cooling runs were measured, and data was collected from the second and third heating run to determine the glass transition temperature.

A cone calorimeter (Fire Testing Technology Ltd., East Grinstead, UK) was used for forced-flaming combustion experiments according to ISO 5660. Samples (100 mm x 100 mm x 4 mm) were stored in a climate control (T = 23 °C; RH = 50%) for at least 48 h before testing. To simulate a developing fire, [27, 28] a distance between sample and heater of 35 mm and a heat flux of 50 kW m^{-2} was chosen. Tests were conducted in duplicate, unless the margin of error was greater than 10%, whereupon a third measurement was conducted.

3. Results and Discussion:

3.1. Synthesis of FRs

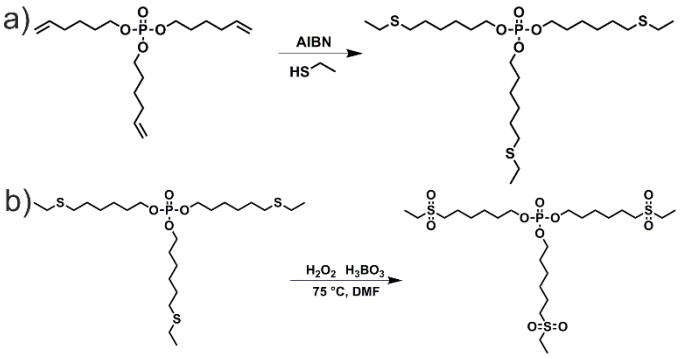

Scheme 1. Synthesis schemes of thio-ether and sulfone-containing FRs: a) mPE and ethanethiol were allowed to react via thiol-ene-reaction with AIBN as initiator to form mPE-S; b) mPE-S was oxidized with hydrogen peroxide with boronic acid as a catalyst to form mPE-S-ox. (SINGLE COLUMN)

mPE was synthesized by the reaction of 5-hexen-1-ol with phosphoryl chloride as previously described.[11]

The synthesis of **mPE-S** was performed in a single reaction step from **mPE** and ethanethiol by a thiol-ene-reaction (Scheme 1 a). Further purification, such as distillation or chromatography, was not necessary. The resulting compound was a liquid at room temperature and had a calculated P-content of 5.84 wt.-%. It was soluble in aromatic (e.g. toluene) and halogenated solvents (e.g. dichloromethane and chloroform), and insoluble in water. Successful synthesis of **mPE-S** was followed by ^{1}H NMR spectroscopy (Figure 1 a). After the thiol-ene-reaction, the resonances of the double bonds at 8.83 – 5.70 ppm and 5.02 – 4.93 ppm vanished, and a new resonance signal at 2.51 ppm for the methylene groups next to the thio-ether was detected. The ^{31}P NMR spectrum (Figure 1 b) revealed a single signal at -0.67 ppm, which is typical for phosphates.

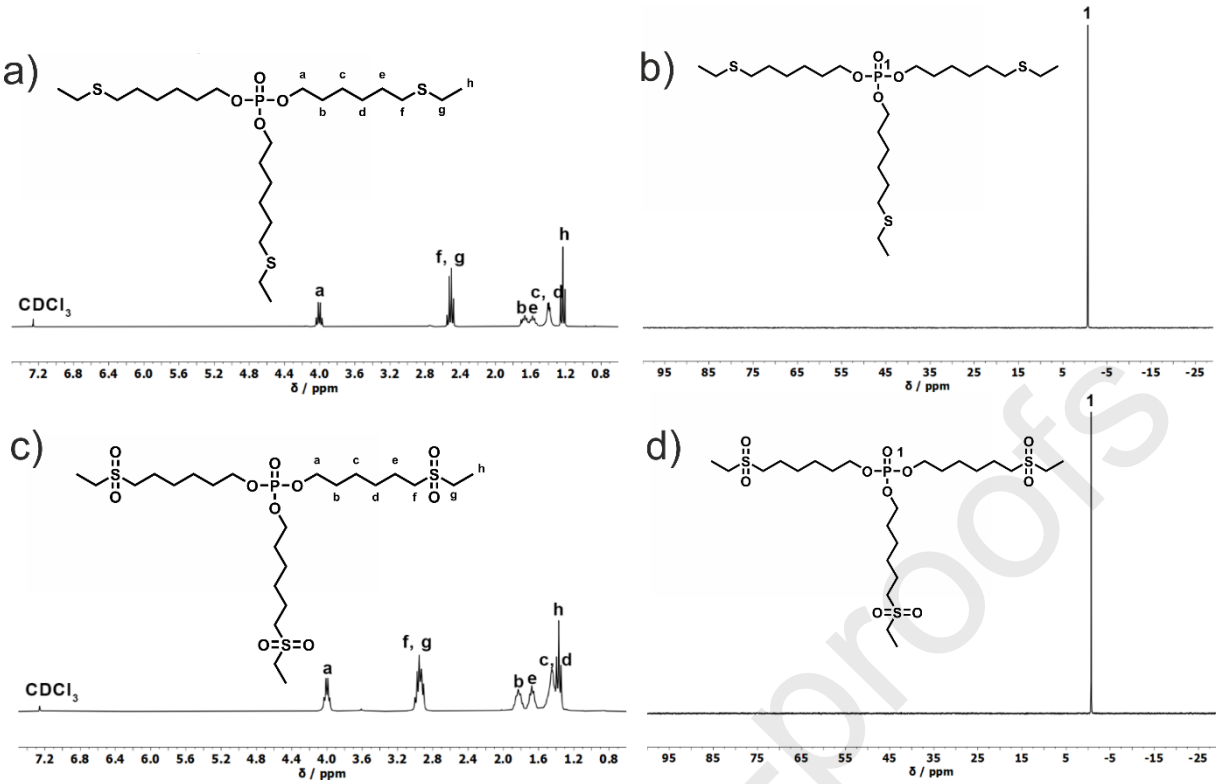

Figure 1. a) ^{1}H NMR (300 MHz in $CDCl_3$ at 298 K) of **mPE-S**; b) ^{31}P {H} NMR (121 MHz in $CDCl_3$ at 298 K) of **mPE-S**; c) ^{1}H NMR (300 MHz in $CDCl_3$ at 298 K) of **mPE-S-ox**; ^{31}P {H} NMR (121 MHz in $CDCl_3$ at 298 K) of **mPE-S-ox**. (2-COLUMN)

In a second reaction, **mPE-S** was oxidized with hydrogen peroxide using boronic acid as a catalyst (Scheme 1 b) at 75 °C overnight to form **mPE-S-ox**. After oxidation to the sulfone, the resonance of the methylene groups next to the sulfone group shifted downfield to 2.95 ppm in ^{1}H NMR (Figure 1 c), which is characteristic and has been reported for similar compounds.[29] In addition, the successful oxidation to the sulfone and not to the sulfoxide was supported by IR spectroscopy, as indicated by the characteristic frequencies at 1299 cm^{-1} and 1124 cm^{-1} (Figure 2 a) [30] and MALDI-TOF mass spectrometry (Figure 2 b).

The polymeric FR **hbPPE** was prepared via a thiol-ene reaction of **mPE** with ethanedithiol. Its synthesis has been previously described and will not be further illustrated here.[10]

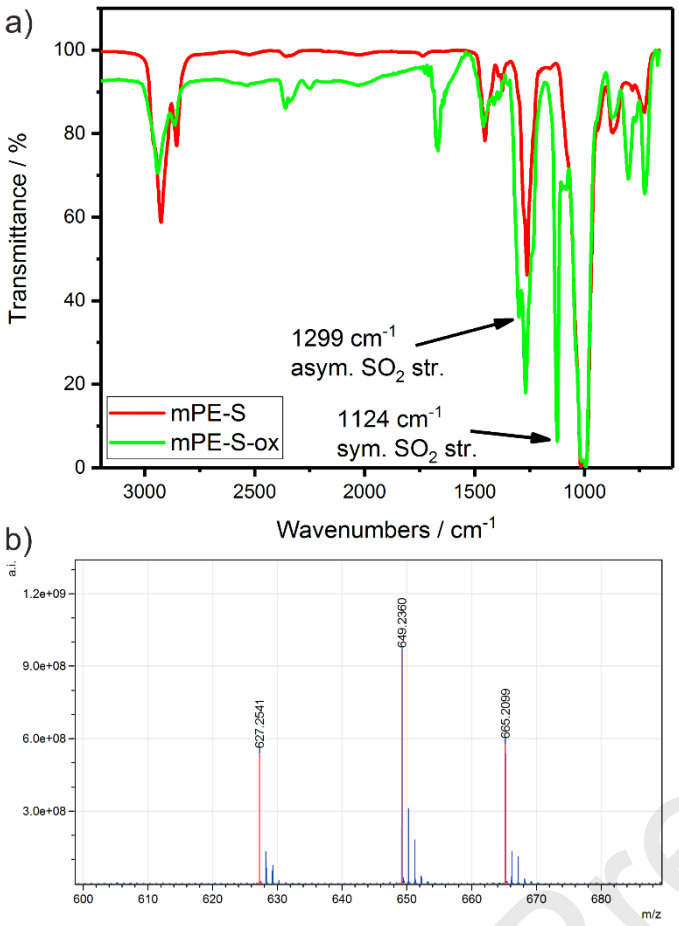

Figure 2. a) FTIR spectra of mPE-S and mPE-S-ox, highlighting the asymmetrical and symmetrical SO_2 stretching frequencies; b) MALDI of mPE-S-ox with DCBT as matrix (left to right: $[M+H]^+$, $[M+Na]^+$, and $[M+K]^+$). (SINGLE COLUMN)

3.2. Pyrolysis – Decomposition Temperature and Mass Loss of FRs

Table 2. Results from thermogravimetric analysis (TGA) of FRs and EP.

Material	$T_{5\%}$ / °C	T_{max} / °C	ML_{max} / wt.-%	$T_{shoulder}$ / °C	$ML_{shoulder}$ / wt.-%	Residue (700°C) / wt.-%
mPE	195 ±3	250 ±2	95.7 ±1.4	–	–	2.8 ±0.8
mPE-S	228 ±4	277 ±0	90.2 ±1.6	–	–	7.5 ±0.2
mPE-S-ox	252 ±4	286 ±2	83.4 ±0.0	–	–	11.8 ±0.5
hbPPE	242 ±2	280 ±1	83.3 ±0.2	–	–	11.2 ±1.4
DGEBA-DMC	338 ±1	372 ±1	62.0 ±0.8	424 ±5	33.2 ±0.3	4.5 ±0.1
BDP	331 ±1	415 ±6	85.5 ±2.2	467 ±3	11.8 ±1.3	1.8 ±0.9

Onset temperatures ($T_{5\%}$); temperature of maximum decomposition rate (T_{max}); mass loss of decomposition step at T_{max} (ML_{max}); temperature of additional decomposition step, i.e. "shoulder" ($T_{shoulder}$); mass loss of decomposition step at shoulder ($ML_{shoulder}$).

All FRs were characterized by their mass loss under pyrolytic conditions via thermogravimetric analysis (TGA) (Table 2). The mass loss and mass loss rate curves of **mPE-S** and **mPE-S-ox** (Figure 3 a) highlighted that both S-FRs are more thermally stable than **mPE**. The beginning of decomposition, i.e. the temperature at 5 wt.-% mass loss ($T_{5\%}$), of **mPE-S** was approx. 30 °C higher than that of **mPE**, and $T_{5\%}$ of **mPE-S-ox** was approx. 10 °C higher than that of **hbPPE**. The temperature of maximum decomposition rate (T_{max}) of **mPE-S** was in the same temperature region as that of **hbPPE**, and **mPE-S-ox** decomposed at slightly higher temperatures (T_{max} = 286 °C). The increased thermal stability stems from the thio-ether or sulfone groups, which are more thermally stable than allyl-groups. By "end-capping" the vinyl groups of **mPE**, added thermal stability is afforded to **mPE-S**. Furthermore, sulfone groups are more thermally stable than thio-ether groups, as **mPE-S-ox** degraded at elevated temperatures compared to **mPE-S**. When comparing the residues at 700 °C, the residue of **mPE-S** was higher than that of **mPE** by a factor of 2.7. Moreover, the residue of **mPE-S-ox** was in the same range as that of **hbPPE**. The presence of thio-ethers altered the decomposition of **mPE** by replacing the highly reactive vinyl group; moreover, the thio-ether bond decomposed to form sulfur radicals. As it has been shown that radical formation plays a significant role in flame retardancy,[31] the higher residue yield is explained by sulfur radicals undergoing cross-linking reaction with the decomposing FR.

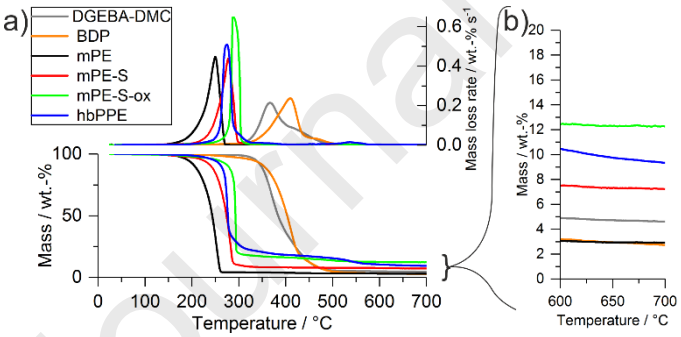

Figure 3. a) Mass loss (bottom) and mass loss rate (top) of pyrolytic decomposition of pure FRs and EP via TGA; b) Comparison of residue remaining between 600 – 700 °C of pure FRs and EP. (SINGLE COLUMN)

3.3. Pyrolysis – Evolved gas analysis of FRs

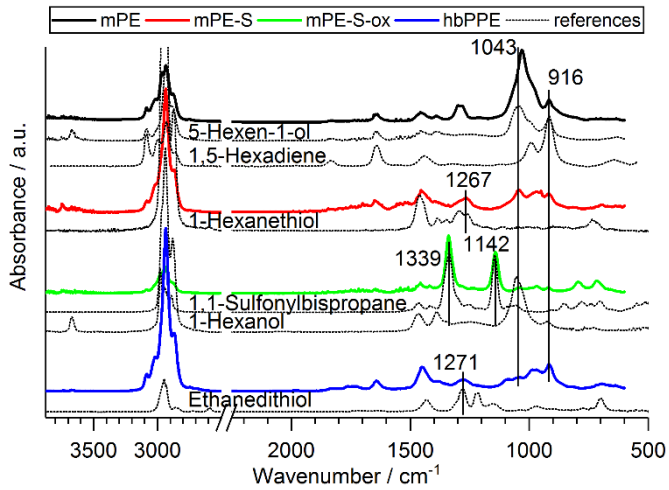

Figure 4. FTIR spectra of pyrolytic decomposition products of FRs at T_{max} via thermogravimetric analysis coupled with Fourier transform infrared spectroscopy (TG-FTIR). (SINGLE COLUMN)

The evolved gases during pyrolytic decomposition were analyzed via thermogravimetric analysis coupled with Fourier transform infrared spectroscopy (FTIR) (Figure 4), and via pyrolysis coupled with gas chromatography and subsequent mass spectrometry (Py-GC/MS) (Figure 5). The decomposition products of **mPE** and **hbPPE** were previously investigated: the main products corresponded to 5-hexen-1-ol, where the ω-OH group was identified via FTIR by the band at 1043 cm^{-1}, and 1,5-hexadiene, where the vinyl group exhibited a strong band at 916 cm^{-1}.[32] The vinyl function, which was visible for all tested FRs, resulted from *cis*-eliminations, where the scission of the (PO)-C bond resulted in an vinyl group.[11] **hbPPE** exhibited an additional absorption band at 1271 cm^{-1} which matched a signal from ethanedithiol,[33] indicating the presence of S in the decomposition spectrum. For **mPE-S**, the FTIR spectrum exhibited an absorption band at 1267 cm^{-1} which was nearly identical to the band seen in **hbPPE** and comparatively 1-hexanethiol.[33] Thus, this band relates to thio-ether or thiol groups. Moreover, the spectrum showed similarities to 5-hexen-1-ol via the band at 1043 cm^{-1}, implying that the decomposition product contained signals of both ω-OH and thio-ether groups caused by the hydrolytic scission of the P-O bond, resulting in the production of 6-(ethylsulfanyl)-1-hexanol. For **mPE-S-ox**, the decomposition spectrum displayed strong absorption at 1339 and 1142 cm^{-1} belonging to characteristic sulfone groups,[32] as evidenced by the comparative spectrum of 1,1-sulfonylbispropane.[33] Furthermore, the development of 1-hexanol was underlined by the absorption at 1043 cm^{-1} and confirmed by Py-GC/MS.

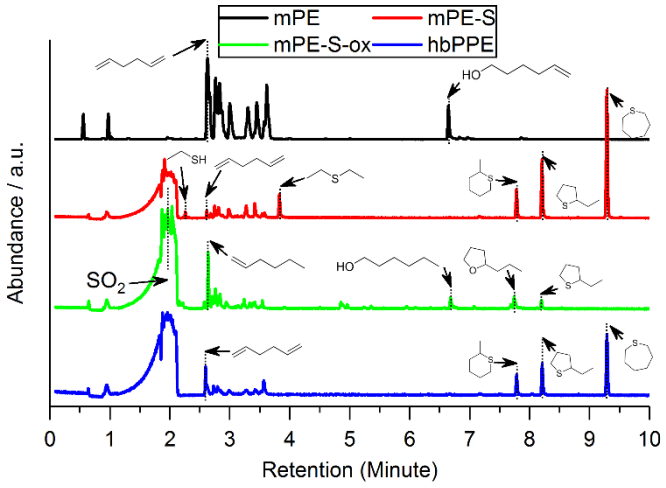

Figure 5. Gas chromatograms of FRs from Pyrolysis-Gas Chromatography/ Mass Spectrometry (Py-GC/MS) measurements. (SINGLE COLUMN)

Py-GC/MS measurements of the FRs (Figure 5) provided further evidence of the evolution of specific decomposition products identified in FTIR spectra of the evolved gases (Figure 4). The presence of 5-hexene-1-ol in the FTIR spectrum of **mPE** was verified in the mass spectrum at a retention time of 6.63 min (Figure S6). For **mPE-S**, the production of ethanethiol at 2.26 min (Figure S2) and diethyl sulfide at 3.38 min (Figure S5) were observed. Identical to **hbPPE**, **mPE-S** decomposed to form tetrahydro-2-methyl-2H-thiopyran (7.79 min, Figure S9), 2-ethyltetrahydro thiophene (8.21 min, Figure S10), and thiepane (9.29 min, Figure S11). Notably, **mPE-S-ox** formed SO_2, as implied by the mass spectrum at 1.92 min (Figure S1), as well as 1-hexanol at 6.68 min (Figure S7). The formation of SO_2 for sulfones has been noted in literature.[17] **mPE-S-ox** decomposed to form a tetrahydrofuran-like material; the mass spectrum of 2-propyl-tetrahydrofuran showed similarities to the mass spectrum at 7.75 min (Figure S8), yet 2-ethyl-tetrahydrofuran is more reasonably formed when considering the C-atom amount. Notably, the mass spectrum at 8.21 min of **mPE-S-ox** shared similarities with 2-ethyltetrahydro thiophene, possibly stemming from unreacted thio-ether groups. The production of 1,5-hexadiene was present in the chromatograms of **mPE**, **mPE-S**, and **hbPPE** at 2.63 min (Figure S3). However, for mPE-S-ox the evolution of 1-hexene was observed at 2.64 min (Figure S4).

The decomposition mechanisms for **mPE**[11] and **hbPPE**[10] have been described previously, and generally involved *cis*-eliminations and hydrolysis reactions. From the evolved gas analyses from FTIR and Py-GC/MS measurements, a decomposition process for the S-FRs is proposed (Scheme 2):

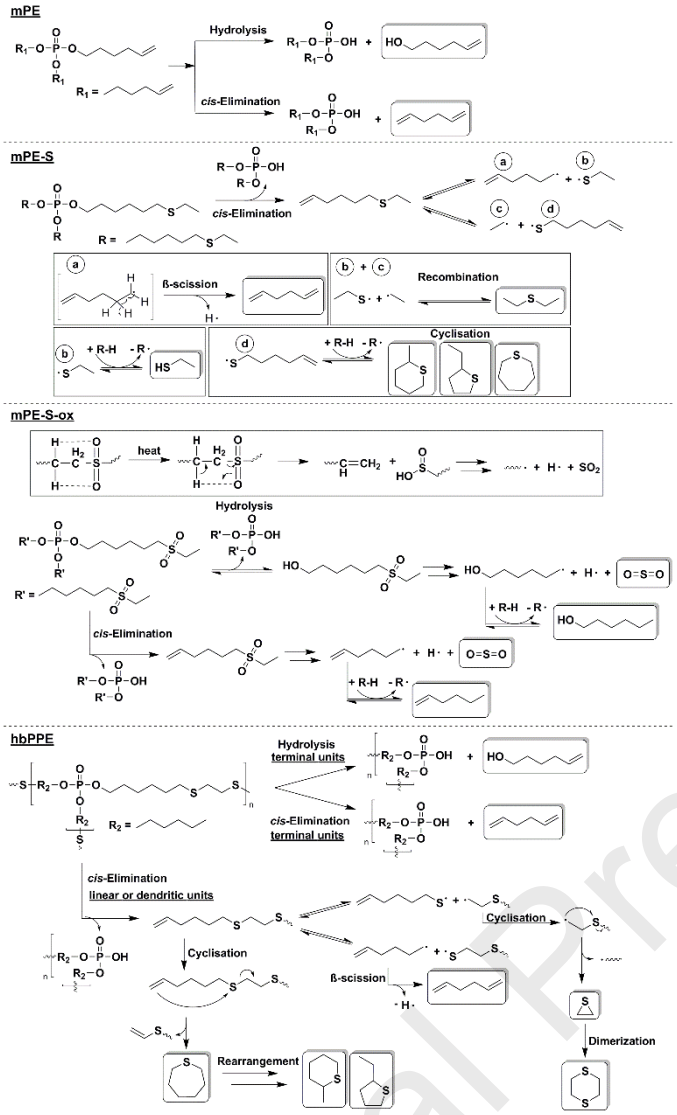

Scheme 2. Proposed decomposition scheme of **mPE**, **mPE-S**, **mPE-S-ox**, and **hbPPE**. Substances in solid boxes were identified in FTIR or Py-GC/MS and comparative spectra. ((SINGLE COLUMN))

The decomposition of several thio-ether[34] and sulfone[35, 36]–containing compounds have been described in literature and involves the production of S-radicals. For **mPE-S**, *cis*-elimination leads to the production of 6-(ethylsulfanyl)-1-hexene, which further decomposes via the homolytic cleavage of the C-S bond, thus producing the products (a), (b), (c), and (d) (Scheme 2), depending on which C-S bond is cleaved. The ß-scission of (a) leads to the formation of 1,5-hexadiene, which was identified in Py-GC/MS, and the recombination reaction of (b) and (c) leads to the formation of diethyl sulfide, which was also detected. Hydrogen atom abstraction of (b) leads to ethanethiol, which was observed at 2.26 min, and hydrogen transfer of (d) and cyclisation reactions lead to the formation of tetrahydro-2-methyl-2H-thiopyran, 2-ethyltetrahydro thiophene, and thiepane. For **mPE-S-ox**, the driving force of decomposition is the release of SO_2: sulfone-containing olefins undergo a transfer of the ß-hydrogen atom to the sulfone-group and subsequent elimination of a vinyl functionalized olefin and sulfinic acid,

the latter rapidly decomposing to form SO_2 and alkyl radicals.[37] Hydrolysis or *cis*-elimination reactions of **mPE-S-ox** form 1-(ethylsulfonyl) hexanol or 1-(ethylsulfonyl)-hex-5-en, respectively. Both products decompose via the aforementioned pathway, and via hydrogen atom transfer reactions 1-hexanol or 1-hexene are produced; both compounds were identified in Py-GC/MS. The decomposition of **hbPPE** is expanded (Scheme 2) to more precisely describe the production of several measured compounds: while hydrolysis or *cis*-elimination reactions of terminal groups lead to the production of 5-hexene-1-ol or 1,5-hexadiene, respectively, *cis*-elimination of linear or dendritic units yields thio-ether-containing compounds. These thio-ethers undergo cyclisation and elimination reactions to form cyclic thio-ethers, but they also undergo homolytic C-S bond cleavage to form radical compounds: the vinyl-functionalized alkyl radical undergoes ß-scission to yield 1,5-hexadiene, and previously reported[10] thiirane and 1,4-dithiane are formed from elimination reactions and subsequent dimerization, respectively.

3.4. Material properties – Resin Blends

In most cases, additives act as plasticizers in polymer resins: additives affect the cross-linking density of the material, altering its mechanical properties and affecting the glass-transition temperature (T_g).[38] The impact of the FRs on the T_g of EP was determined via differential scanning calorimetry (DSC) (Figure 6 a) DGEBA-DMC had a T_g of 155 °C, and the addition of FRs lowered it between 21 – 38 °C (Figure 6 b). EP with BDP (**EP/BDP**) had a T_g of ca. 134 °C; EP with **hbPPE** (**EP/hbPPE**) and EP with **mPE-S-ox** (**EP/mPE-s-ox**) displayed T_gs in a similar temperature range, i.e. 132 and 129 °C, respectively. Resins with **mPE** (**EP/mPE**) and **mPE-S** (**EP/mPE-S**) exhibited the lowest T_gs at 117 and 118 °C, respectively. DSC measurements identified that the thio-ether-containing **mPE-S** affected the T_g of EP similarly to the allyl-functionalized **mPE**, indicating that "end-capping" did not improve the impact on T_g. Furthermore, the sulfone-containing **mPE-S-ox** had a reduced impact on T_g of EP, comparable to that of **hbPPE**. This phenomenon can be explained by the bulky sulfone groups that affect the free-volume of the matrix, thus altering the energy needed to attain a flowing process of the polymer chain, resulting in increased T_g.[39]

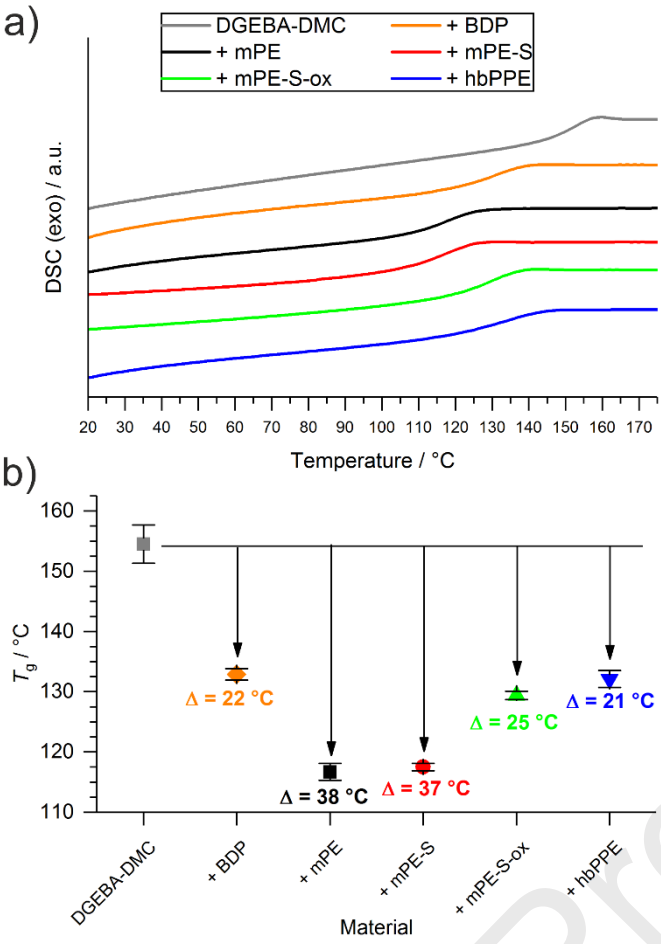

Figure 6. a) Differential scanning calorimetry (DSC) measurements of the second heating run of EP and EP-FRs; b) Relative change in glass-transition temperature (T_g) of EP-FRs compared to EP. (SINGLE COLUMN)

3.5. Pyrolysis – Decomposition Temperature and Mass Loss of Resin Blends

The pyrolytic decomposition of EP and EP-FRs were investigated via TGA (Figure 7 a): the mass loss of EPs with S-FRs illustrated that the low $T_{5\%}$ and approx. 10 wt.-% mass loss near 230 °C exhibited by **EP/mPE** was not shared by **EP/mPE-S** or **EP/mPE-S-ox** (Table 2), implying that "end-capping" the vinyl-groups increased the thermal stability of the EP-FRs. This is further exemplified by the low T_{max} of **EP/mPE** compared to the S-FR-containing EPs; T_{max} of **EP/mPE-S** and of **EP/mPE-S-ox** were both in the same range as T_{max} of **EP/BDP** and of **EP/hbPPE**, i.e. about 15 – 20 °C lower than T_{max} of EP. Moreover, the residue yields at 700 °C of S-FR-containing FRs were higher than that of **EP/mPE** (Figure 7 b). The addition of **mPE** to resins increased residue yields at 700 °C by about 13%, which is the lowest among the tested FRs. However, **mPE-S-ox** and **mPE-S** had a greater impact on residue, increasing yields by 41% compared to pure EP (residue = 4.5 wt.-%). When comparing **EP/mPE** to the S-FRs, the thio-ether "end-capping" led to an increase in residue yield of 24% (Table S1). The sulfone-containing FR did not additionally yield higher residues compared to the thio-ether. The presence of sulfur increased the thermal stability of **mPE**, leading to increased interaction with the decomposing matrix, thus producing

higher char yields. Moreover, the presence of sulfur in FRs may promote cross-linking reactions by generating sulfur-radicals, as noted in the decomposition of the pure FRs. The oxidation state of sulfur did not play a role in the increase of residue. EP with **hbPPE** exhibited higher pyrolytic residues than those EPs with low molar mass S-FRs, even though pure **mPE-S-ox** had similar residue yields as pure **hbPPE**. The presence of sulfur in FRs improved the residue yields of EP in pyrolysis, thus helping to explain the high residue yields of **EP/hbPPE**. Additionally, the presence of certain S-species may act as a synergist with P-based flame retardants; previous investigations into halogenated flame retardants for polystyrene proved some cooperative effects of disulfides and sulfonamides.[40]

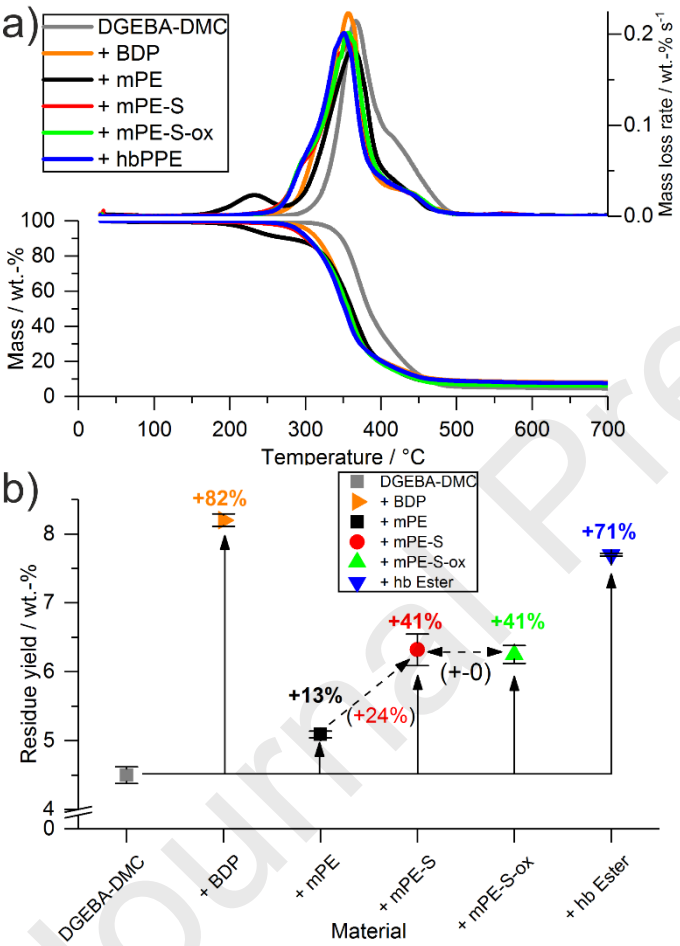

Figure 7. a) Mass loss (bottom) and mass loss rate (top) versus temperature via thermogravimetric analysis (TGA); b) Change in residue yields at 700 °C of EP-FRs compared to EP. (SINGLE COLUMN)

3.6. Pyrolysis – Evolved gas analysis of Resin Composites

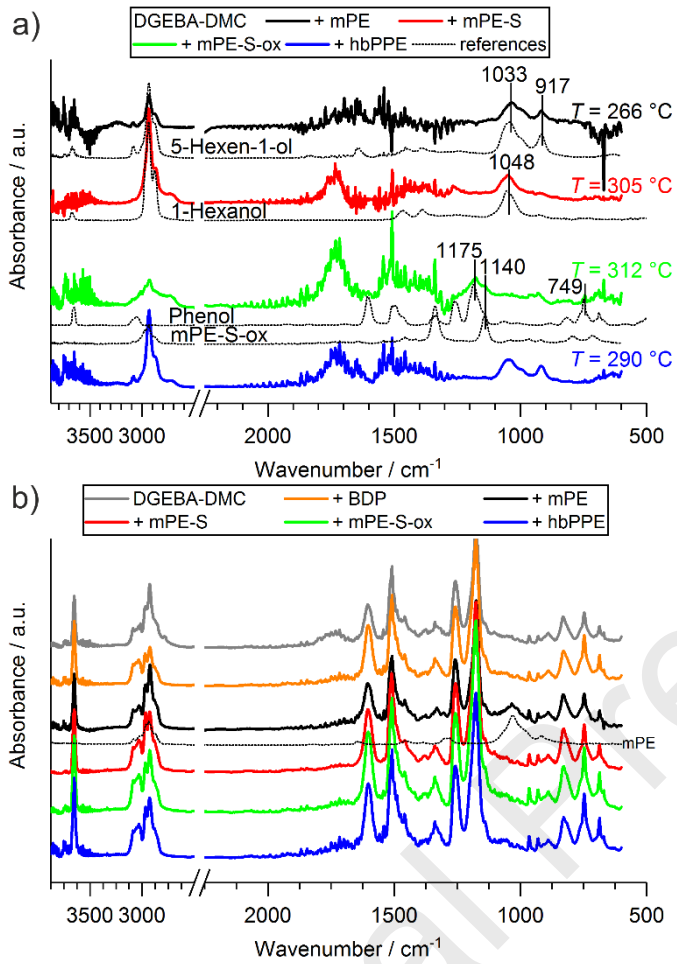

Figure 8. TG-FTIR spectra of pyrolytic decomposition products at a) decomposition step prior to main step, and at b) main decomposition step. (SINGLE COLUMN)

Evolved gas analysis of the resin blends further illustrated the FR modes of action: FTIR analysis of the pyrolytic decomposition products (Figure 8) highlighted the evolution of specific products prior to the main decomposition step (Figure 8 a), namely 5-hexen-1-ol for **EP/mPE** and **EP/hbPPE**. For **EP/mPE-S**, the spectrum shared similarities with 1-hexanol, especially via the absorption band at 1048 cm^{-1} and the lack of absorption at 917 cm^{-1} which corresponds to δ_{oop}(C-H) of the vinyl groups. The spectrum of **EP/mPE-S-ox** at 312 °C exhibited decomposition products from the epoxy matrix, especially from phenol products, identified by the absorption bands at 1175 and 749 cm^{-1}. Moreover, the spectrum shares similarities with the evolved gas of pure **mPE-S-ox**, as identified by the band at 1140 cm^{-1} belonging to $\nu_s(SO_2)$, thus implying that some SO_2-species progressed into the gas phase. The spectra at the main decomposition step (Figure 8 b) showed the decomposition of the epoxy matrix, as evidenced by the similarities of all spectra with that of EP. As previously reported, [11] the spectrum

of **EP/mPE** exhibited **mPE** signals even at the main decomposition step, most probably due to phosphorylation of the resin caused by the strong reactivity of **mPE**.

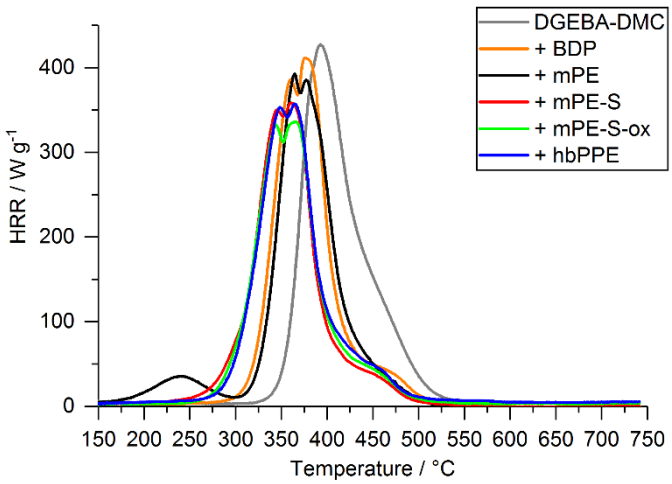

Figure 9. Heat release rates over time of EP and EP-FRs from pyrolysis combustion flow calorimetry (PCFC). (SINGLE COLUMN)

The resin blends were analyzed by means of pyrolysis combustion flow calorimetry (PCFC) to further understand how the evolved gas affects the gas phase. Although some FRs are known to act in the gas phase via radical scavenging, this mode of action cannot be detected in PCFC due to the complete oxidation of the pyrolysis products in the combustion zone. However, PCFC (otherwise known as micro cone calorimetry, i.e. MCC) may be used to measure fuel dilution effects, as the evolution of incombustible gases do not contribute to oxygen consumption, i.e. heat release. The production of incombustible gases can be quantified by changes in the heat of complete combustion (h_c^0). The plot of HRR vs. time (Figure 9) of PCFC measurements pointed to a decrease in PHRR for most flame retardant-containing EPs, with **mPE-S-ox** lowering the PHRR of EP by 21% (340 W g^{-1}, as opposed to 429 W g^{-1} of EP). **EP/mPE-S-ox** also displayed the lowest heat release capacity (HRC), THE, and h_c^0, followed by **EP/mPE-S** (Table S2). The low molar mass S-FRs produced incombustible products during pyrolytic decomposition: For **mPE-S-ox**, SO_2-release was identified in Py-GC/MS measurements, and PCFC results of **EP/mPE-S-ox** further illuminate that its release is a gas-phase mode of action of this FR. Moreover, **mPE-S** produced a S-containing compound during pyrolysis, i.e. 1-hexanethiol or a derivative thereof. As this product further decomposed, it produced incombustible gases, as indicated by the reduction in h_c^0. Notably, **hbPPE** did not have the same effect in lowering h_c^0 as **mPE-S** or **mPE-S-ox** in **EP**; this is mainly due to the presence of linear and terminal units in the structure of **hbPPE**, which decomposed to form 1,5-hexadiene, analogous to **mPE**. The release of this compound contributed to the combustion heat, thus explaining the increase in h_c^0 for **EP/mPE** compared to EP.

Thus, the thio-ether groups competed with the vinyl-groups in **hbPPE**, leading to only moderate reduction in h_c^0 of **EP/hbPPE** comprated to EP.

3.7. Pyrolysis – Condensed Phase Activity of Resin Blends

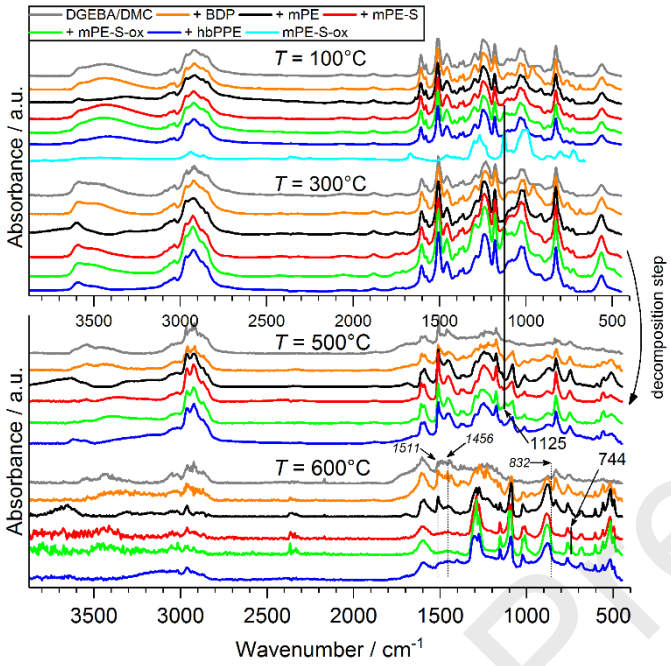

Figure 10. Condensed phase FTIR spectra from hot stage FTIR measurements of EP and EP-FRs at specific temperatures (100, 300, 500, 600 °C). Dotted lines/ italic numbers: bands not present in S-FRs.

(SINGLE COLUMN)

The condensed phase spectra from hot-stage FTIR measurements (Figure 10) portrayed the change in specific absorption bands for all FR-containing EP blends. For **EP/mPE-S-ox**, the band of asymmetrical $\nu(SO_2)$ was visible at 1125 cm^{-1} between 100 – 500 °C, indicating its presence even after the main decomposition step of EP. Moreover, both **EP/mPE-S** and **EP/mPE-S-ox** exhibited an absorption band at 744 cm^{-1} at 600 °C, which correspond to S-containing species such as ν(C-S) of O=CH-S-Ar, ν_s(S-O-C) of S-O-CH_2-R, or ν_s(P=S) of various P and S-containing compounds.[30, 32] The spectra of the S-containing EP-FRs and **EP/hbPPE** did not exhibit absorption bands at 1511, 1456 and 832 cm^{-1}, where EP, **EP/mPE**, and **EP/BDP** showed signals. These bands originate from Bisphenol A-based compounds; their disappearance for **EP/mPE-S**, **EP/mPE-S-ox**, and **EP/hbPPE** indicates that S-FRs have a different decomposition pathway.

While the volatility of the low molar mass FRs was significantly reduced after thiol-ene reaction and oxidation (cf. TGA measurements in Figure 3), the additional thio-ethers or sulfons affected the FR's

reactivity. Phosphorylation is a major contributor to the condensed phase mode of action of P-FRs: the interaction between hydroxyl groups in the resin matrix and P-species leads to increased charring.[41] However, this process changed when polar groups such as thio-ether or sulfone were present. Thus, although all FR are active in the condensed phase and S-containing FRs exhibited higher residue amounts in EP in pyrolysis measurements (Table 3), the type of residue is notably different from sulfur-free to sulfur-containing FRs. It has been reported that the production of sulfonic acid further promotes char formation.[42, 43] The presence of S-containing species may point to such a process for the tested FRs.

3.8. Fire Testing of Resin Blends

Fire testing via cone calorimeter measurements was effective in examining the modes of action of the various FRs and especially the S-FRs. From the results (Table 3), a reduction of the total heat evolved (THE = total heat release [THR] at flame-out) of all EP-FRs was noted, although the degree of reduction was distinct for each FR. **mPE** had the strongest impact on reducing the fire load of EP, lowering THE by 28% (Figure 11 b). The S-FRs **mPE-S-ox** and **mPE-S** exhibited a less pronounced fire load reduction of EP, only lowering its THE by 8 and 11%, respectively, whereas the benchmark FR **BDP** and the hyperbranched polymeric FR **hbPPE** both lowered THE of EP by 17 and 19%, respectively. The HRR curves (Figure 11 a) shed some light on the modes of action of the low molar mass S-FRs: About 30 s after ignition, the curves of **EP/mPE** and **EP/hbPPE** exhibited a reduction in HRR and displayed a plateau-like area resultant from the formation of a protective char layer. This plateau was also visible for **EP/mPE-S** and **EP/mPE-S-ox**, but the reduction in HRR was less pronounced; furthermore, the peak of heat release rate (PHRR) of **EP/mPE-S-ox** was higher than that of **EP/mPE-S**, indicating that the protective layer effect was stronger for the thio-ether-containing FR than for the sulfone-containing one. This point was strengthened by the fact that **EP/mPE-S** and **EP/hbPPE** had similar PHRR values; both contain thio-ether groups. The changes to THE and PHRR can be visualized via Petrella-plot, where the fire load, i.e. THE, is plotted versus the fire growth index, i.e. PHRR/ time to ignition (t_{ig}) (Figure 11 c).[44] Both low molar mass S-FRs were able to lower fire load and fire growth index of EP in a similar manner, with **mPE-S** lowering THE of EP more strongly. However, **mPE** and **hbPPE** were more effective in lowering the fire load and fire growth rate of EP, illustrating that these materials were more able to bind fuel or create a strong protective layer than the S-FRs. This is further exemplified by the residue yields: while all FRs increased char yields (Figure 11 d), **EP/mPE-S-ox** had the second lowest char yield of all tested materials, the lowest exhibited by **EP/BDP**. Moreover, the char yield of **EP/mPE-S** was in a similar range to that of **EP/hbPPE**, further highlighting that thio-ether-containing FRs were more effective in storing fuel in the form of carbonaceous char than sulfone-containing FRs in EP blends. The S-FRs were able to create higher residue amounts in pyrolytic investigations of EP than during fire tests,

and the low char yield also helps explain the higher fire loads of **EP/mPE-S** and **EP/mPE-S-ox** compared to the other EP-FRs. The low char yield in fire tests resulted from a reduced phosphorylation of the matrix, i.e. a low reactivity of the FR's decomposition products with the decomposing matrix. Moreover, **mPE-S** and **mPE-S-ox** have a lower P-content than **mPE** or **hbPPE** (Table 1), thus explaining the lower residue yields and higher fire loads in EP blends resulting from a reduced P-based condensed and gas phase activity. Fire tests proved that the high volatility and reactivity of **mPE**, as well as its higher P-content, was more effective in binding fuel compared to the thio-ether and sulfone-containing FRs. As evolved gas analysis highlighted the production of SO_2 for the sulfone-containing FR, its gas diluting effect may be the main mode of action; however, it is plausible that the release of SO_2 inhibited the FR to effectively bind fuel in the condensed phase. Furthermore, the reduced P-content of **mPE-S-ox** further explains the lower residue yield and protective layer effect in EP, as well as a higher fire load.

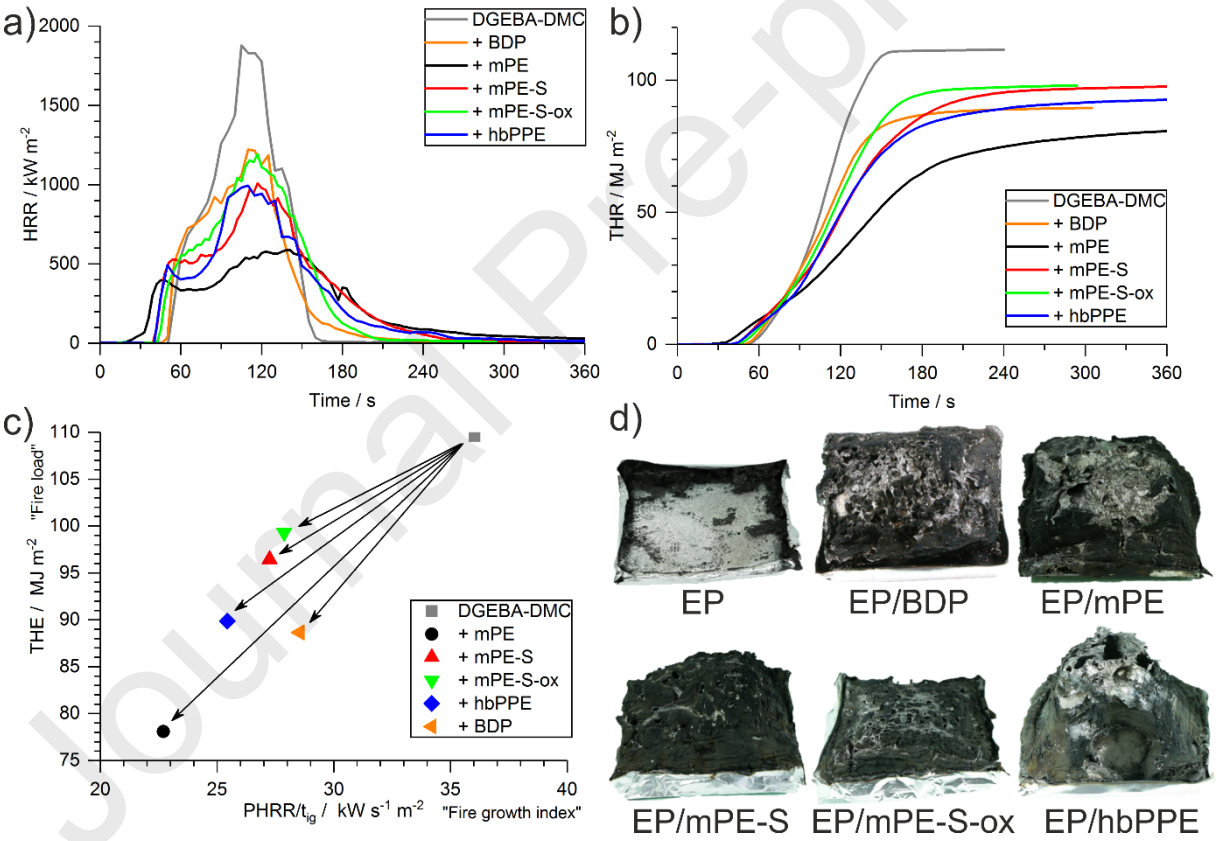

Figure 11. a) Heat release rate (HRR) versus time of EP and EP-FRs; b) Total heat release (THR) versus time of EP and EP-FRs; c) Petrella-plot of EP and EP-FRs; d) Residue photographs (10 cm x 10 cm aluminum tray base) of EP and EP-FRs after cone calorimeter measurements. (2-COLUMN)

Table 3. Results from cone calorimeter measurements.

	THE / MJ m^{-2}	PHRR / kW m^{-2}	μ / wt.-%	EHC / MJ kg^{-1}
EP	108.4 ±2.6	1696 ±180	0.7 ±0.1	26.9 ±1.0
EP/BDP	87.5 ±1.2	1180 ±41	3.1 ±0.2	22.7 ±0.2
EP/mPE	78.1 ±6.5	885 ±16	9.2 ±0.1	21.6 ±1.8
EP/mPE-S	96.5 ±0.7	958 ±51	7.7 ±0.0	25.2 ±0.6
EP/mPE-S-ox	99.3 ±5.0	1219 ±26	4.7 ±0.5	27.5 ±0.4
EP/hbPPE	89.8 ±3.0	953 ±41	7.5 ±0.6	24.3 ±0.6

Total heat evolved (THE = total heat released at flame-out); peak of heat release rate (PHRR); char yield (μ); effective heat of combustion (EHC).

4. Conclusion

To gain further insight into the flame-retardant effect of polymeric hyperbranched poly(phosphoesters) **hbPPE**, the material was compared to two sulfur-containing low molar mass variants of the monomeric phosphoester **mPE**.

Pyrolytic decomposition investigations of the FRs illustrated that the increased thermal stability and higher residue yield of **hbPPE** compared to its monomer **mPE** stemmed not only from its higher molecular mass, but also from thio-ether groups present in **hbPPE**: the thio-ether-containing FR **mPE-S** displayed a higher T_{dec} and residue yield than **mPE**, and the sulfone-containing **mPE-S-ox** proved even more thermally stable and retained higher residues than **mPE-S**. The presence of sulfur altered the decomposition pathway of the P-FRs: thio-ethers promoted the production of S-radicals which cross-linked to promote residue yield, while sulfonates decomposed to release incombustible SO_2.

In epoxy resins, the sulfur-containing FRs affected the glass-transition temperature of the resin less strongly than the sulfur-free **mPE**. Moreover, the presence of sulfur decreased the volatility of the P-FRs and encouraged an overlap of decomposition temperatures of FR and matrix, thus improving chemical reactivity. Moreover, the presence of sulfur increased condensed phase activity, and several sulfur species were identified in the residues via FTIR. Fire tests of FR-containing epoxy resins exemplified that **hbPPE**'s effectiveness as an FR was not rooted solely in the presence thio-ether groups, but the occurrence of both vinyl and thio-ether groups.

The results of this study highlight that the presence of sulfur in **hbPPE** played a significant role to the multifunctional qualities of the hyperbranched P-FR, mainly by improving thermal stability, reducing

the impact on T_g of epoxy resins, and adding additional chemical decomposition mechanisms in the condensed phase and thus improving residue yields.

5. Acknowledgements

Funding: This work was supported by the Deutsche Forschungsgemeinschaft [DFG SCHA 730/15-1; DFG WU 750/8-1].

Alexander Battig thanks Dr. Katharina Kebelmann (BAM) for help with Py-GC/MS measurements and Patrick Klack (BAM) for support with the cone calorimeter. Jens C. Markwart is the recipient of a fellowship through funding of the Excellence Initiative (DFG/ GSC 266) in the context of the graduate school of excellence "MAINZ" (Materials Science in Mainz). Frederik R. Wurm and Jens C. Markwart thank Prof. Dr. Katharina Landfester (MPIP) for support.

6. Data Availability

The raw/processed data required to reproduce these findings may be delivered upon request.

7. References

[1] M.M. Velencoso, A. Battig, J.C. Markwart, B. Schartel, F.R. Wurm, Molecular Firefighting-How Modern Phosphorus Chemistry Can Help Solve the Challenge of Flame Retardancy, Angew Chem Int Edit, 57 (2018) 10450-10467.
[2] Q.F. Wang, W.F. Shi, Kinetics study of thermal decomposition of epoxy resins containing flame retardant components, Polymer Degradation and Stability, 91 (2006) 1747-1754.
[3] C.J. Hawker, J.M.J. Frechet, Preparation of Polymers with Controlled Molecular Architecture - a New Convergent Approach to Dendritic Macromolecules, Journal of the American Chemical Society, 112 (1990) 7638-7647.
[4] Q. Cao, P.S. Liu, Hyperbranched polyurethane as novel solid-solid phase change material for thermal energy storage, European Polymer Journal, 42 (2006) 2931-2939.
[5] A. Asif, W.F. Shi, Synthesis and properties of UV curable waterborne hyperbranched aliphatic polyester, European Polymer Journal, 39 (2003) 933-938.
[6] B.I. Voit, A. Lederer, Hyperbranched and Highly Branched Polymer Architectures-Synthetic Strategies and Major Characterization Aspects, Chemical Reviews, 109 (2009) 5924-5973.
[7] C.R. Yates, W. Hayes, Synthesis and applications of hyperbranched polymers, European Polymer Journal, 40 (2004) 1257-1281.
[8] F. Marsico, A. Turshatov, R. Pekoz, Y. Avlasevich, M. Wagner, K. Weber, D. Donadio, K. Landfester, S. Baluschev, F.R. Wurm, Hyperbranched Unsaturated Polyphosphates as a Protective Matrix for Long-Term Photon Upconversion in Air, Journal of the American Chemical Society, 136 (2014) 11057-11064.
[9] K. Täuber, F. Marsico, F.R. Wurm, B. Schartel, Hyperbranched poly(phosphoester)s as flame retardants for technical and high performance polymers, Polym Chem-Uk, 5 (2014) 7042-7053.
[10] A. Battig, J. Markwart, F.R. Wurm, B. Schartel, Hyperbranched Phosphorus Flame Retardants: Multifunctional Additives for Epoxy Resins, Polym Chem-Uk, 10 (2019) 4346-4358.

[11] J.C. Markwart, A. Battig, L. Zimmermann, M. Wagner, J. Fischer, B. Schartel, F.R. Wurm, Systematically Controlled Decomposition Mechanism in Phosphorus Flame Retardants by Precise Molecular Architecture: P–O vs P–N, ACS Applied Polymer Materials, 1 (2019) 1118-1128.
[12] B.A. Howell, Y.G. Daniel, The impact of sulfur oxidation level on flame retardancy, Journal of Fire Sciences, 36 (2018) 518-534.
[13] S.V. Levchik, E.D. Weil, Overview of recent developments in the flame retardancy of polycarbonates, Polymer International, 54 (2005) 981-998.
[14] J. Green, Mechanisms for Flame Retardancy and Smoke suppression -A Review, Journal of Fire Sciences, 14 (1996) 426-442.
[15] W. Pawelec, A. Holappa, T. Tirri, M. Aubert, H. Hoppe, R. Pfaendner, C.E. Wilen, Disulfides - Effective radical generators for flame retardancy of polypropylene, Polymer Degradation and Stability, 110 (2014) 447-456.
[16] J. Wagner, P. Deglmann, S. Fuchs, M. Ciesielski, C.A. Fleckenstein, M. Döring, A flame retardant synergism of organic disulfides and phosphorous compounds, Polymer Degradation and Stability, 129 (2016) 63-76.
[17] U. Braun, U. Knoll, B. Schartel, T. Hoffmann, D. Pospiech, J. Artner, M. Ciesielski, M. Döring, R. Perez-Gratero, J.K.W. Sandler, V. Altstädt, Novel phosphorus-containing poly(ether sulfone)s and their blends with an epoxy resin: Thermal decomposition and fire retardancy, Macromolecular Chemistry and Physics, 207 (2006) 1501-1514.
[18] C.L. Rasmussen, P. Glarborg, P. Marshall, Mechanisms of radical removal by SO2, P Combust Inst, 31 (2007) 339-347.
[19] M.R. Zachariah, O.I. Smith, Experimental and Numerical-Studies of Sulfur Chemistry in H2-O2-So2 Flames, Combustion and Flame, 69 (1987) 125-139.
[20] R.M. Perez, J.K.W. Sandler, V. Altstädt, T. Hoffmann, D. Pospiech, M. Ciesielski, M. Döring, U. Braun, A.I. Balabanovich, B. Schartel, Novel phosphorus-modified polysulfone as a combined flame retardant and toughness modifier for epoxy resins, Polymer, 48 (2007) 778-790.
[21] M. Lewin, Flame retarding of polymers with sulfamates .1. Sulfation of cotton and wool, Journal of Fire Sciences, 15 (1997) 263-276.
[22] M. Lewin, J. Brozek, M.M. Martens, The system polyamide/sulfamate/dipentaerythritol: Flame retardancy and chemical reactions, Polymers for Advanced Technologies, 13 (2002) 1091-1102.
[23] M. Lewin, J. Zhang, E. Pearce, J. Gilman, Flammability of polyamide 6 using the sulfamate system and organo-layered silicatet, Polymers for Advanced Technologies, 18 (2007) 737-745.
[24] J.Y. He, G. Cai, C.A. Wilkie, The effects of several sulfonates on thermal and fire retardant properties of poly(methyl methacrylate) and polystyrene, Polymers for Advanced Technologies, 25 (2014) 160-167.
[25] W. Zhao, B. Li, M.J. Xu, L.L. Zhang, F.M. Liu, L.M. Guan, Synthesis of a novel flame retardant containing phosphorus and sulfur and its application in polycarbonate, Polym Eng Sci, 52 (2012) 2327-2335.
[26] Y.H. Chen, H.Q. Peng, J.H. Li, Z.X. Xia, H. Tan, A novel flame retardant containing phosphorus, nitrogen, and sulfur, Journal of Thermal Analysis and Calorimetry, 115 (2014) 1639-1649.
[27] B. Schartel, T.R. Hull, Development of fire-retarded materials - Interpretation of cone calorimeter data, Fire and Materials, 31 (2007) 327-354.
[28] B. Schartel, M. Bartholmai, U. Knoll, Some comments on the main fire retardancy mechanisms in polymer nanocomposites, Polymers for Advanced Technologies, 17 (2006) 772-777.
[29] M.S.F. Lie Ken Jie, O. Bakare, 1H- and 13C-NMR studies on sulfinyl and sulfonyl derivatives of positional isomers of methyl thialaurate, Chem. Phys. Lipids, 61 (1992) 139-147.
[30] G. Socrates, Infrared and Raman characteristic group frequencies: tables and charts, John Wiley & Sons, 2004.
[31] G. Camino, L. Costa, Performance and Mechanisms of Fire Retardants in Polymers - a Review, Polymer Degradation and Stability, 20 (1988) 271-294.
[32] M. Hesse, H. Meier, B. Zeeh, Spektroskopische Methoden in der organischen Chemie, Georg Thieme Verlag, 2005.

[33] P.J. Linstrom, Mallard, W.G., NIST Standard Reference Database Number 69, in, 2018.
[34] J.P. Machon, A. Nicco, Thermal Decomposition Reactions of Oligomeric Thioethers of Polythioethene and Polythiotrimethylene, European Polymer Journal, 7 (1971) 1693-&.
[35] F. Vögtle, L. Rossa, Pyrolysis of Sulfones as a Synthetic Method, Angewandte Chemie-International Edition in English, 18 (1979) 515-529.
[36] E. Wellisch, E. Gipstein, O.J. Sweeting, Thermal decomposition of polysulfones, Journal of Applied Polymer Science, 8 (1964) 1623-1631.
[37] E. Wellisch, O.J. Sweeting, E. Gipstein, Thermal Decomposition of Sulfinic Acids, J Org Chem, 27 (1962) 1810-&.
[38] M. Ciesielski, B. Burk, C. Heinzmann, M. Döring, Fire-retardant high-performance epoxy-based materials, in: D.-Y. Wang (Ed.) Novel Fire Retardant Polymers and Composite Materials, Woodhead Publishing, 2017, pp. 3-51.
[39] J.M.G. Cowie, V. Arrighi, Polymers: chemistry and physics of modern materials, CRC press, 2007.
[40] J. Eichhorn, Synergism of free radical initiators with self-extinguishing additives in vinyl aromatic polymers, Journal of Applied Polymer Science, 8 (1964) 2497-2524.
[41] B. Schartel, B. Perret, B. Dittrich, M. Ciesielski, J. Krämer, P. Müller, V. Altstädt, L. Zang, M. Döring, Flame Retardancy of Polymers: The Role of Specific Reactions in the Condensed Phase, Macromolecular Materials and Engineering, 301 (2016) 9-35.
[42] A. Ballistreri, G. Montaudo, E. Scamporrino, C. Puglisi, D. Vitalini, S. Cucinella, Intumescent Flame Retardants for Polymers .4. The Polycarbonate Aromatic Sulfonates System, J Polym Sci Pol Chem, 26 (1988) 2113-2127.
[43] A. Nodera, T. Kanai, Thermal decomposition behavior and flame retardancy of polycarbonate containing organic metal salts: Effect of salt composition, Journal of Applied Polymer Science, 94 (2004) 2131-2139.
[44] R. Petrella, The assessment of full-scale fire hazards from cone calorimeter data, Journal of fire sciences, 12 (1994) 14-43.

8. Figure Captions

Scheme 1. Synthesis schemes of thio-ether and sulfone-containing FRs: a) mPE and ethanethiol were allowed to react via thiol-ene-reaction with AIBN as initiator to form mPE-S; b) mPE-S was oxidized with hydrogen peroxide with boronic acid as a catalyst to form mPE-S-ox. (SINGLE COLUMN)

Scheme 2. Proposed decomposition scheme of **mPE**, **mPE-S**, **mPE-S-ox**, and **hbPPE**. Substances in solid boxes were identified in FTIR or Py-GC/MS and comparative spectra. (SINGLE COLUMN)

Figure 1. a) ^{1}H NMR (300 MHz in $CDCl_3$ at 298 K) of **mPE-S**; b) ^{31}P {H} NMR (121 MHz in $CDCl_3$ at 298 K) of **mPE-S**; c) ^{1}H NMR (300 MHz in $CDCl_3$ at 298 K) of **mPE-S-ox**; ^{31}P {H} NMR (121 MHz in $CDCl_3$ at 298 K) of **mPE-S-ox**. (2-COLUMN)

Figure 2. a) FTIR spectra of mPE-S and mPE-S-ox, highlighting the asymmetrical and symmetrical SO_2 stretching frequencies; b) MALDI of mPE-S-ox with DCBT as matrix (left to right: $[M+H]^+$, $[M+Na]^+$, and $[M+K]^+$). (SINGLE COLUMN)

Figure 3. a) Mass loss (bottom) and mass loss rate (top) of pyrolytic decomposition of pure FRs and EP via TGA; b) Comparison of residue remaining between 600 – 700 °C of pure FRs and EP. (SINGLE COLUMN)

Figure 4. FTIR spectra of pyrolytic decomposition products of FRs at T_{max} via thermogravimetric analysis coupled with Fourier transform infrared spectroscopy (TG-FTIR). (SINGLE COLUMN)

Figure 5. Gas chromatograms of FRs from Pyrolysis-Gas Chromatography/ Mass Spectrometry (Py-GC/MS) measurements. (SINGLE COLUMN)

Figure 6. a) Differential scanning calorimetry (DSC) measurements of the second heating run of EP and EP-FRs; b) Relative change in glass-transition temperature (T_g) of EP-FRs compared to EP. (SINGLE COLUMN)

Figure 7. a) Mass loss (bottom) and mass loss rate (top) versus temperature via thermogravimetric analysis (TGA); b) Change in residue yields at 700 °C of EP-FRs compared to EP. (SINGLE COLUMN)

Figure 8. TG-FTIR spectra of pyrolytic decomposition products at a) decomposition step prior to main step, and at b) main decomposition step. (SINGLE COLUMN)

Figure 9. Heat release rates over time of EP and EP-FRs from pyrolysis combustion flow calorimetry (PCFC). (SINGLE COLUMN)

Figure 10. Condensed phase FTIR spectra from hot stage FTIR measurements of EP and EP-FRs at specific temperatures (100, 300, 500, 600 °C). Dotted lines/ italic numbers: bands not present in S-FRs. (SINGLE COLUMN)

Figure 11. a) Heat release rate (HRR) versus time of EP and EP-FRs; b) Total heat release (THR) versus time of EP and EP-FRs; c) Petrella-plot of EP and EP-FRs; d) Residue photographs (10 cm x 10 cm aluminum tray base) of EP and EP-FRs after cone calorimeter measurements. (2-COLUMN)

Table of Contents

"Sulfur's Role in the Flame Retardancy of Thio-Ether–linked Hyperbranched Poly(phosphoesters) in Epoxy Resins"

Alexander Battig,[a,‡] Jens C. Markwart,[b,c,‡] Frederik R. Wurm,*[,b] and Bernhard Schartel*[,a]

[a] Bundesanstalt für Materialforschung und -prüfung (BAM), Unter den Eichen 87, 12205 Berlin, Germany.
[b] Max Planck Institute for Polymer Research, Ackermannweg 10, 55128 Mainz, Germany.
[c] Graduate School Materials Science in Mainz, Staudinger Weg 9, 55128 Mainz, Germany.
[‡] these authors contributed equally

* corresponding authors:
Bernhard Schartel, Bundesanstalt für Materialforschung und -prüfung (BAM), Unter den Eichen 87, 12205 Berlin, Germany. bernhard.schartel@bam.de;
Frederik R. Wurm, Max-Planck-Institut für Polymerforschung, Ackermannweg 10, 55128 Mainz, Germany. wurm@mpip-mainz.mpg.de

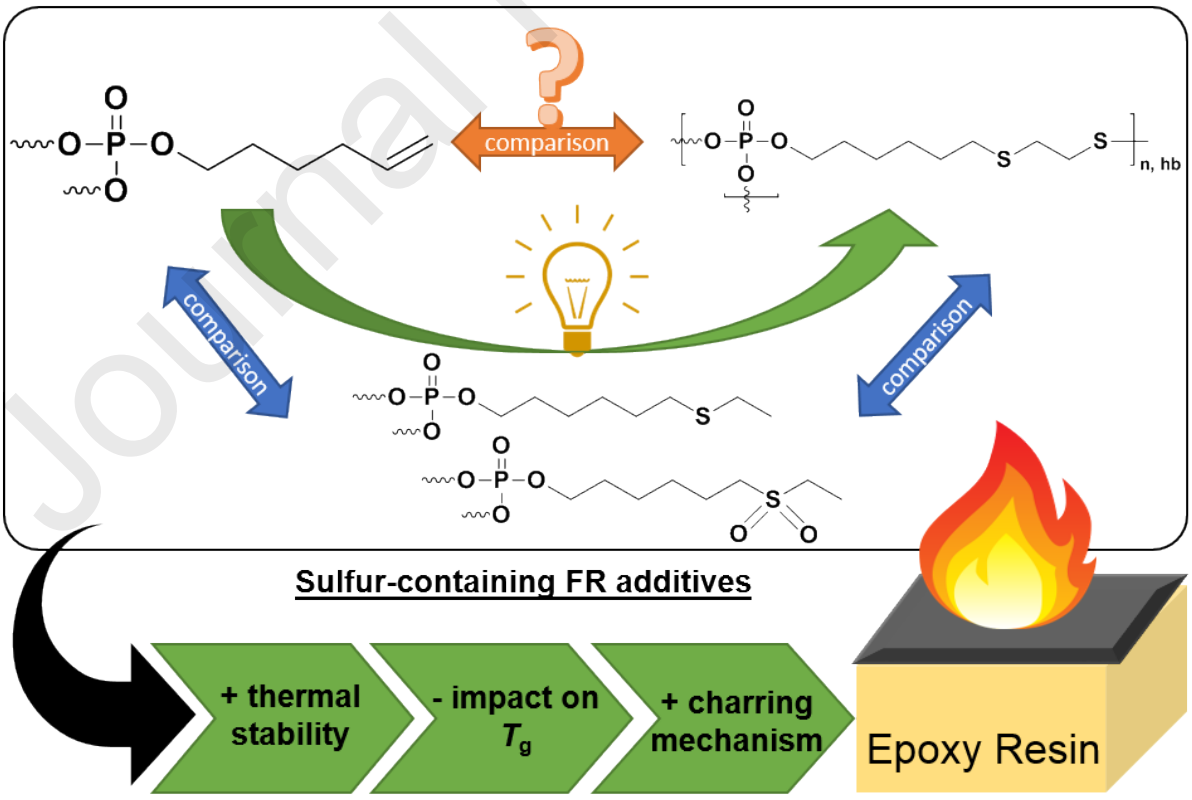

Declaration of interests

☒ The authors declare that they have no known competing financial interests or personal relationships that could have appeared to influence the work reported in this paper.

☐The authors declare the following financial interests/personal relationships which may be considered as potential competing interests:

Author Contributions

Sulfur's Role in the Flame Retardancy of Thio-Ether–linked Hyperbranched Poly(phosphoesters) in Epoxy Resins

Alexander Battig,[a,‡] Jens C. Markwart,[b,c,‡] Frederik R. Wurm,[*,b] and Bernhard Schartel[*,a]

[a] Bundesanstalt für Materialforschung und -prüfung (BAM), Unter den Eichen 87, 12205 Berlin, Germany.

[b] Max Planck Institute for Polymer Research, Ackermannweg 10, 55128 Mainz, Germany.

[c] Graduate School Materials Science in Mainz, Staudinger Weg 9, 55128 Mainz, Germany.

[‡] these authors contributed equally

* corresponding authors:

Bernhard Schartel, Bundesanstalt für Materialforschung und -prüfung (BAM), Unter den Eichen 87, 12205 Berlin, Germany. bernhard.schartel@bam.de;

Frederik R. Wurm, Max-Planck-Institut für Polymerforschung, Ackermannweg 10, 55128 Mainz, Germany. wurm@mpip-mainz.mpg.de

Alexander Battig: Conceptualization, Methodology, Investigations, Writing – Original Draft preparation; Writing – Review & Editing, Visualization; **Jens C. Markwart**: Investigations, Resources, Writing-Original Draft preparation; **Frederik R. Wurm:** Conceptualization, Supervision, Funding Acquisition; Writing–Review and Editing; **Bernhard Schartel:** Conceptualization, Supervision, Funding Acquisition; Writing–Review and Editing